

# Seismic imaging of magma sills beneath an ultramafic-hosted hydrothermal system

# J. Pablo Canales<sup>1</sup>, Robert A. Dunn<sup>2</sup>, Ryuta Arai<sup>3</sup>, and Robert A. Sohn<sup>1</sup>

<sup>1</sup>Department of Geology and Geophysics, Woods Hole Oceanographic Institution, Woods Hole, Massachusetts 02543, USA <sup>2</sup>Department of Geology and Geophysics, University of Hawaii at Manoa, Honolulu, Hawaii 96822, USA

## **ABSTRACT**

Hydrothermal circulation at mid-ocean ridge volcanic segments extracts heat from crustal magma bodies. However, the heat source driving hydrothermal circulation in ultramafic outcrops, where mantle rocks are exhumed in low-magma-supply environments, has remained enigmatic. Here we use a three-dimensional P-wave velocity model derived from active-source wide-angle refraction-reflection ocean bottom seismometer data and pre-stack depth-migrated images derived from multichannel seismic reflection data to investigate the internal structure of the Rainbow ultramafic massif, which is located in a non-transform discontinuity of the Mid-Atlantic Ridge. Seismic imaging reveals that the ultramafic rocks composing the Rainbow massif have been intruded by a large number of magmatic sills, distributed throughout the massif at depths of  $\sim$ 2–10 km. These sills, which appear to be at varying stages of crystallization, can supply the heat needed to drive high-temperature hydrothermal circulation, and thus provide an explanation for the hydrothermal discharge observed in this ultramafic setting. Our results demonstrate that high-temperature hydrothermal systems can be driven by heat from deep-sourced magma even in exhumed ultramafic lithosphere with very low magma supply.

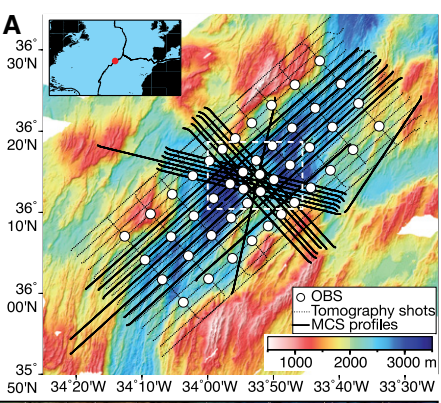
### INTRODUCTION

Exposures of mantle rocks are common along mid-ocean ridges spreading at slow to ultraslow rates (<55 mm/yr), especially in magma-poor regions (e.g., Tucholke and Lin, 1994). Hydrothermal circulation at these sites produces serpentine via the reaction of seawater with ultramafic rocks (e.g., Allen and Seyfried, 2004), resulting in fluids enriched in H<sub>2</sub>, CH<sub>4</sub>, and other abiogenic hydrocarbons (e.g., Holm and Charlou, 2001). Where exit-fluid temperatures are low (<100 °C), hydrothermal circulation can be sustained by a combination of exothermic serpentinization and heat mined from hot lithosphere (e.g., Allen and Seyfried, 2004). However, a magmatic heat source is required to explain hydrothermal circulation at ultramafic sites where fluids exit the seafloor at high flow rates and elevated temperatures (>340 °C) and are enriched in CO<sub>2</sub> (Allen and Seyfried, 2004), despite these systems being located in settings away from neovolcanic zones such as ridge-axis discontinuities (German et al., 1996), rift valley walls (e.g., Ondreas et al., 2012), and inside-corner highs (Okino et al., 2015). While magma systems beneath volcanic-hosted hydrothermal sites are well characterized (e.g., Singh et al., 1999), the heat sources that drive high-temperature hydrothermal systems in ultramafic settings have yet to be imaged. As a result, we have no in situ constraints on the geometry of

the subsurface circulation system, and an incomplete understanding of the relationship between lithospheric accretion, extension and hydrothermal processes in ultramafic environments.

#### **GEOLOGICAL SETTING**

The Rainbow ultramafic massif is thought to be an oceanic core complex (OCC) formed by detachment faulting (Andreani et al., 2014) within a non-transform discontinuity (NTD) of the Mid-Atlantic Ridge (MAR; Fig. 1). The massif hosts the Rainbow hydrothermal field (RHF) (German et al., 1996), which vents fluids enriched in CH4, H2, and Fe (diagnostic of serpentinization; Holm and Charlou, 2001) at high temperatures and flow rates (German et al., 2010), indicating that a magmatic heat source is present (Allen and Seyfried, 2004). However, the tectonized setting of the NTD lacks significant volcanic features (Andreani et al., 2014; Eason et al., 2016; Paulatto et al., 2015). The massif is largely covered by pelagic sediments, but basement outcrops expose predominately serpentinites, with sparse occurrence of plutonic rocks and basalts (Andreani et al., 2014). The presence of two inactive hydrothermal sites (Ghost City and Clamstone; Fig. 1B) is inferred from fossil evidence (Lartaud et al., 2010, 2011), but neither of them shows evidence of past hightemperature activity (Andreani et al., 2014).



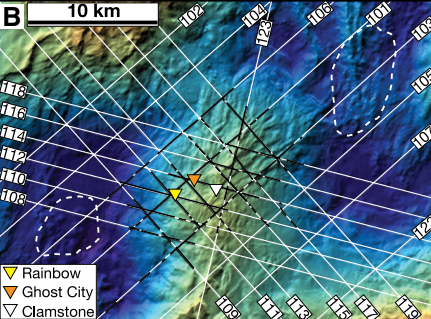


Figure 1. A: Regional bathymetry (Paulatto et al., 2015) and layout of the seismic experiment across the Rainbow non-transform discontinuity (NTD) and neighboring segments. Dashed white box shows location of maps shown in B and Figure 2A. White dots—ocean bottom seismometers (OBS); MCS—multichannel seismic. Inset shows location. B: Bathymetry of the Rainbow NTD. Labeled white lines are MCS profiles; black segments show locations where sills have been imaged. Triangles indicate hydrothermal sites. Closed white contours locate areas of elevated seafloor magnetization (Paulatto et al., 2015).

# NEW GEOPHYSICAL DATA AND METHODS

To understand how magmatic and tectonic processes give rise to high-temperature hydrothermal activity in an ultramafic setting we conducted a geophysical investigation of the Rainbow NTD and neighboring segments using shipboard acoustic and potential fields (Paulatto et al., 2015; Eason et al., 2016), and

<sup>&</sup>lt;sup>3</sup>Research and Development Center for Earthquake and Tsunami, Japan Agency for Marine-Earth Science and Technology, Yokohama, Kanagawa, Japan

active-source seismic imaging. We used traveltimes of *P*-waves recorded by 43 ocean bottom seismometers (OBSs) (Fig. 1A) using an iterative technique to compute the three-dimensional (3-D) *P*-wave velocity (*V*p) structure (Dunn et al., 2005). The 3-D tomography model was used to depth migrate 2-D multichannel seismic (MCS) reflection data collected with an 8-km-long hydrophone streamer along 21 profiles (Fig. 1). Details about the seismic modeling and processing are given in the GSA Data Repository<sup>1</sup>.

### RESULTS AND DISCUSSION

# P-wave Velocity Structure

The 3-D tomography model shows large *V*p variations within the study area (Figs. 2A and 2B). The Rainbow massif is underlain by a coneshaped core of high-*V*p mantle material that is elongated in the northeast-southwest direction (Figs. 2A and 2C). Above this core, the flanks of the massif and adjacent nodal basins are characterized by layers of low to moderately low *V*p (Figs. 2A and 2B) consistent with serpentinite or high-porosity basalts. The lower velocities on the flanks of the massif are most likely associated with highly serpentinized peridotites, based on seafloor samples (Andreani et al., 2014).

#### **Pre-Stack Depth-Migrated Images**

Seismic reflection images reveal two primary types of events within the massif: reflectors beneath both flanks of the massif that dip at 35°–45° away from the area where hydrothermal venting is clustered near the summit of the massif (Fig. 2D), and short, subhorizontal reflectors broadly distributed throughout the massif confined between the northwest- and southeast-dipping reflectors (Figs. 2C, 3, and 4A).

# Nature of Dipping Reflectors

The dipping reflectors are associated with the boundaries between the high-Vp core of the massif and the overlaying lower velocity layers (Fig. 2D). This indicates that the high-Vp core is separated from the overlaying layers by sharp impedance contrasts that may be produced by faulting, alteration, or lithological contacts. In cross section the dipping reflectors resemble normal faults (Fig. 2D), but their depth extent (~5 km below seafloor, bsf, below the adjacent nodal basin in some instances; Fig. 2D) would require the presence of exposed faults scarps on both flanks of the massif with kilometer-scale vertical throws. Because such scarps are not observed

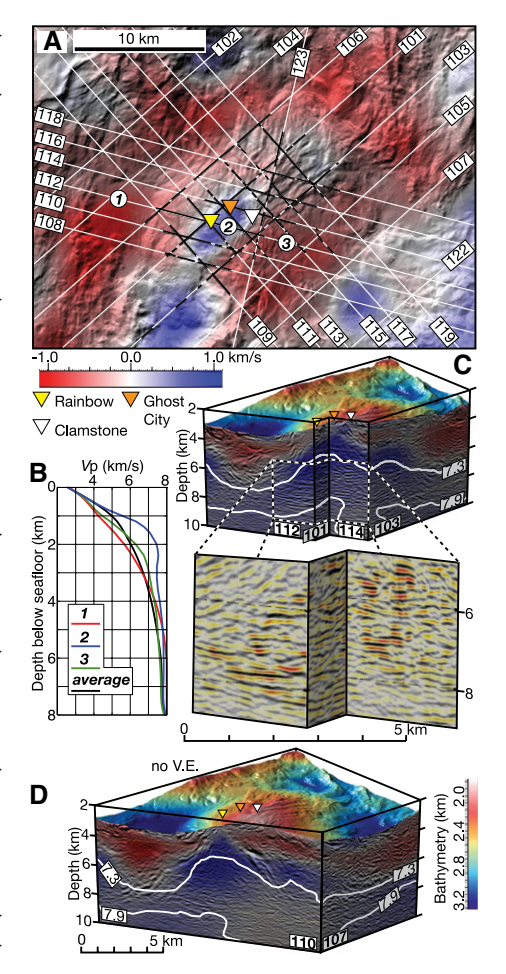


Figure 2. A: Shaded topography of the Rainbow non-transform discontinuity (NTD) colored according to P-wave velocity variations relative to average of the study area (black line in B) at 1 km below seafloor. Circled numbers locate the one-dimensional P-wave velocity (Vp) profiles shown in B. Other symbols as in Figure 1B. B: Vp plotted against depth. C: Perspective views of the Rainbow massif and subseafloor seismic structure. Fence diagram shows sill reflectors beneath both the active Rainbow hydrothermal field (line 112) and the inactive Clamstone and Ghost City sites (line 114), highlighted in the zoomed-in panel. D: Line 110 shows prominent west- and east-dipping reflectors coincident with large lateral variations in seismic velocity. All seismic images show reflectivity overlaid on Vp relative to average (red-blue color scale as in A). White lines show the 7.3 (~20% serpentinization) and 7.9 km/s (fresh peridotite) isovelocity contours. V.E.—vertical exaggeration.

(Andreani et al., 2014; Paulatto et al., 2015), the dipping reflectors most likely represent lithological contacts, serpentinization fronts, or a combination of both. The cone-shaped high-Vp core forms an inverted funnel that shoals beneath the southwest flank near the summit of the massif where hydrothermal activity is clustered (Fig. 2A), indicating that hydrothermal outflow zones may be to some extent controlled by the subseafloor lithological and alteration structure.

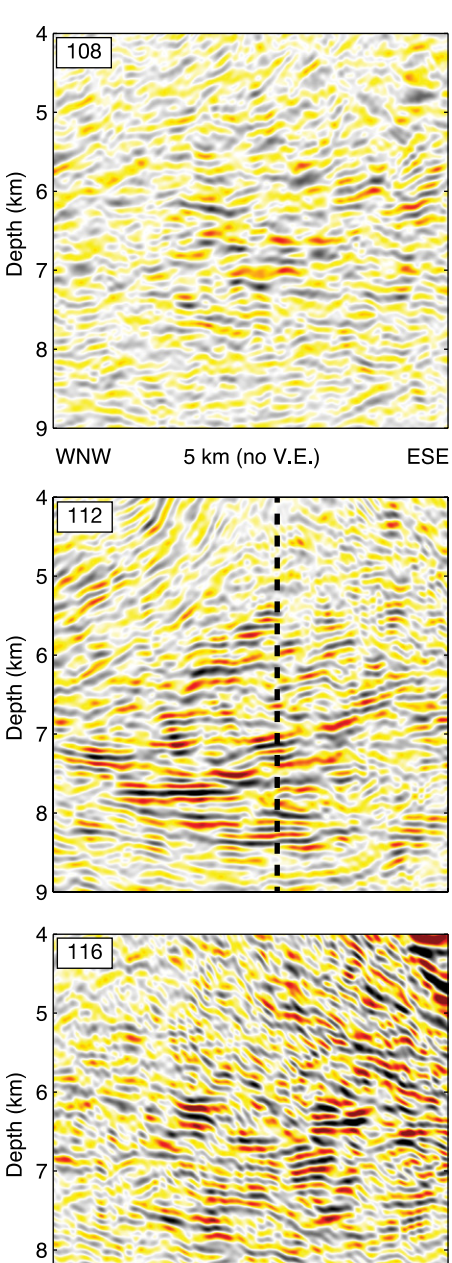


Figure 3. Close-up views of subhorizontal reflectors interpreted as sills across the southwest flank (line 108), center (112), and the northeast flank of the Rainbow massif (116). Dashed line locates the Rainbow hydrothermal field (RHF). V.E.—vertical exaggeration.

# Magma Sills Driving Ultramafic-Hosted Hydrothermal Circulation

The subhorizontal reflectors occupy an area of ~4.6 km × 8 km (Figs. 1B and 4A), and are distributed within a depth range from ~2 to 10 km bsf (the majority are 3–6 km bsf; Fig. 4B). Their appearance and geometry are very similar to those of melt lenses imaged in young crust at other spreading centers (e.g., Marjanović et al., 2014; Nedimović et al., 2005), leading to the conclusion that they represent magmatic sills.

<sup>&</sup>lt;sup>1</sup>GSA Data Repository item 2017134, additional information and images about the geophysical dataset, tomography modeling and checkerboard tests, MCS processing and interpretation, and details about calculations of the energy balance of the Rainbow hydrothermal field, is available online at www.geosociety.org/datarepository/2017 or on request from editing@geosociety.org.

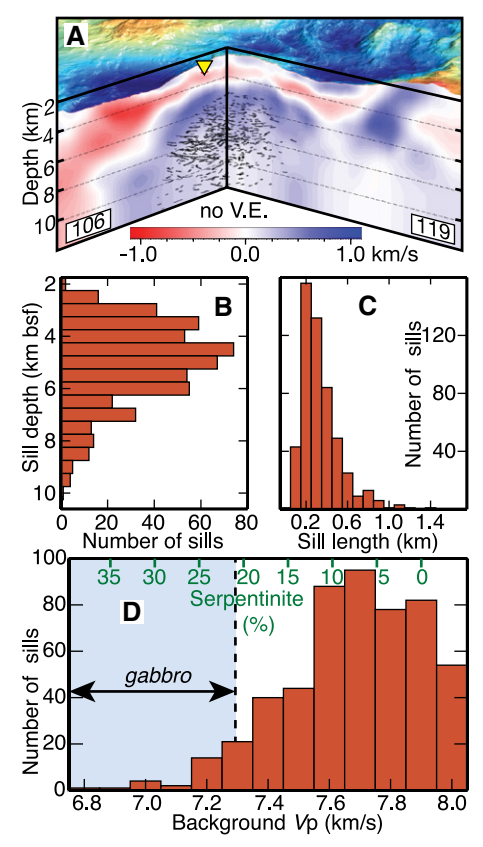


Figure 4. Distribution and characteristics of sills. A: Three-dimensional distribution of sills within the Rainbow massif shown against the relative *P*-wave velocity (*V*p) along profiles 106 and 119. Inverted triangle locates the Rainbow hydrothermal field (RHF). V.E.—vertical exaggeration. B: Histogram shows the distribution of sill depth (bsf—below seafloor). C: Histogram shows the distribution of sill length. D: Vp and inferred degree of serpentinization at the locations of the imaged sills. Values <7.3 km/s may correspond to gabbro matrix or >20% serpentinized peridotite. Values >7.3 km/s correspond to ultramafic rocks that are <20% serpentinized.

The majority of them intrude material with Vp > 7.5 km/s; this implies an ultramafic nature with little or no alteration due to serpentinization (<15%; Fig. 4C). Only a few sills are imaged within material with Vp = 6.8-7.3 km/s, which could correspond to 20%-40% serpentinite, gabbros, or a mixture of both (Fig. 4C).

Our 3-D Vp model does not have the resolution to resolve the small-scale structure of individual sills. However, the sills located closer to the RHF are, in general, of larger dimensions and have larger reflection amplitudes (relative to surrounding reflectivity) than those located farther away (Fig. 3). This, and the high temperature of the RHF fluids, thus suggests that the sills located beneath the vent field are most likely partially molten intrusions that provide the heat to drive hydrothermal circulation, while the rest of the sills are likely solidified. Our MCS data can image both partially molten and solidified

intrusions because they are emplaced within a high *V*p matrix, and thus generate a negative impedance contrast with their host rock (Figs. 2C, 4A, and 4D). The presence of low-*V*p sills may result in underestimation of the tomographically derived background *V*p, but we quantify this effect to be no more than 0.2 km/s (see the GSA Data Repository<sup>1</sup>).

Using previous estimates of heat flux and duration of hydrothermal activity at the RHF (see the Data Repository), we find that the heat delivered by solidification of the imaged sills could cumulatively support high-temperature hydrothermal circulation for a period of ~1600-3000 yr, which is ~7%-30% of the total hydrothermal system lifespan (Cave et al., 2002; Kuznetsov et al., 2006). These estimates approximately double if additional heat, released by crystallization of melt impregnating peridotites that is not accounted for in the seismically imaged sills, is factored in (Table DR3). By comparison, high-temperature discharge at the longer lived, volcanic-hosted TAG active hydrothermal field has been estimated to occur during only 1%-2% of the system lifespan (Humphris and Cann, 2000). Our results thus suggest that the RHF has a greater timeaveraged rate of hydrothermal discharge than the TAG field, which may explain why the massive sulfide deposits at the RHF have structural and mineralogical characteristics comparable to those of the TAG field (Marques et al., 2007), despite being a younger system.

# Sill Intrusions in the Upper Mantle at NTDs

The lateral dimensions of the sills (a few hundred meters to ~1400 m in length; the majority are 200–400 m long; Fig. 4C) and the ultramafic nature of the host rock that they intrude present a scenario similar to the Moho transition zone in ophiolites, where gabbroic sills that are tens to hundreds of meters long and 0.1-100 m thick intrude ultramafic host rock (Boudier et al., 1996; Kelemen and Aharonov, 1998). Small gabbroic bodies intruding ultramafic outcrops are also observed along other portions of the MAR (e.g., Dick et al., 2008), and if emplacement is rapid enough and sustained over sufficiently long periods of time, then thick gabbroic crustal sections may be accreted (Grimes et al., 2008). At the Rainbow massif, however, the sills we image occupy 4.8–9.2 km<sup>3</sup> (assuming a sill thickness of 80-150 m), which is only 1%–2% of the volume of the exhumed ultramafic material (defined as material at depths <8 km bsf and with Vp > 7.3 km/s). This suggests that sill emplacement at the Rainbow massif is slow compared to OCCs with large gabbroic cores (e.g., Grimes et al., 2008), perhaps because of its location within an axial discontinuity.

Exhumation of OCCs involves flexural rotation of the detachment footwall (Garcés and Gee, 2007). Our observation of subhorizontal

sills at the Rainbow massif thus implies that if the massif was exhumed along a detachment fault in a manner similar to that of other OCCs (Andreani et al., 2014), then the sills must have been emplaced after, or at the very end of, footwall rotation and exhumation. This interpretation is consistent with the idea that exhumation of an OCC is terminated by magma emplacement into the footwall (MacLeod et al., 2009). Alternatively, if sill emplacement has occurred throughout the formation of the Rainbow massif, our observations indicate that the massif has not been significantly rotated during exhumation. This scenario could be possible if the massif was exhumed due to buoyancy forces resulting from the volume increase associated with serpentinization (O'Hanley, 1992). The tectonic setting of the Rainbow massif, located within an NTD, could result in different deformation and exhumation mechanisms compared to OCCs formed at segment centers or inside corners, but we do not currently have enough information to address this hypothesis.

Our experiment did not resolve a potential low-Vp source region for the magmatic sills that intrude the massif, a region that is commonly observed beneath volcanic spreading segments (Dunn et al., 2000). The source region for the sills must thus either be deeper than the region that our seismic tomography experiment can resolve (>8 km bsf), or located within the neighboring spreading segments (German and Parson, 1998), thus requiring lateral magma propagation. The lack of a volcanic magnetization signature on the massif (Paulatto et al., 2015) argues against lateral emplacement of the sills, as do the sill depths (~3-6 km bsf), because dikes propagating laterally from a segment center into an NTD are predicted to shoal toward the segment end and breach the seafloor (Behn et al., 2006). The high-magnetization volcanic cones and ridges located at the ends of the neighboring segments (Paulatto et al., 2015) (Fig. 1B) probably mark the loci of maximum dike propagation along these segments. The most plausible magma source region is thus directly beneath the massif, with melt migrating vertically through the upper mantle into the NTD. Our results thus provide compelling evidence that deep-sourced magma can intrude exhumed ultramafic lithosphere to drive hydrothermal circulation even in highly tectonized regions with low long-term magma supply.

#### ACKNOWLEDGMENTS

This research was funded by National Science Foundation (NSF) grants OCE-0961680 and OCE-0961151. We thank the captain, crew, and technical staff of the RV *M.G. Langseth*, and the NSF-funded Ocean Bottom Seismograph Instrument Pool (OBSIP, http://www.obsip.org) managers and technical staff for their efforts, which made possible the success of cruise MGL1305. OBSIP data are archived at the IRIS Data Management Center (Incorporated Research Institutions for Seismology; http://www.iris.edu). MCS field

data are archived with the IEDA Marine Geoscience Data System (doi:10.1594/IEDA/320244).

#### REFERENCES CITED

- Allen, D.E., and Seyfried, W.E., 2004, Serpentinization and heat generation: Constraints from Lost City and Rainbow hydrothermal systems: Geochimica et Cosmochimica Acta, v. 68, p. 1347–1354, doi:10.1016/j.gca.2003.09.003.
- Andreani, M., Escartín, J., Delacour, A., Ildefonse, B., Godard, M., Dyment, J., Fallick, A.E., and Fouquet, Y., 2014, Tectonic structure, lithology, and hydrothermal signature of the Rainbow massif (Mid-Atlantic Ridge 36°14'N): Geochemistry, Geophysics, Geosystems, v. 15, p. 3543–3571, doi:10.1002/2014GC005269.
- Behn, M.D., Buck, W.R., and Sacks, I.S., 2006, Topographic controls on dike injection in volcanic rift zones: Earth and Planetary Science Letters, v. 246, p. 188–196, doi:10.1016/j.epsl.2006.04.005.
- Boudier, F., Nicolas, A., and Ildefonse, B., 1996, Magma chambers in the Oman ophiolite: Fed from the top and the bottom: Earth and Planetary Science Letters, v. 144, p. 239–250, doi:10.1016 /0012-821X(96)00167-7.
- Cave, R.R., German, C.R., Thomson, J., and Nesbitt, R.W., 2002, Fluxes to sediments underlying the Rainbow hydrothermal plume at 36°14′N on the Mid-Atlantic Ridge: Geochimica et Cosmochimica Acta, v. 66, p. 1905–1923, doi:10.1016/S0016-7037(02)00823-2.
- Dick, H.J.B., Tivey, M.A., and Tucholke, B.E., 2008, Plutonic foundation of a slow-spread ridge segment: Oceanic core complex at Kane megamullion, 23°30'N, 45°20'W: Geochemistry, Geophysics, Geosystems, v. 9, Q05014, doi:10.1029 /2007GC001645.
- Dunn, R.A., Toomey, D.R., and Solomon, S.C., 2000, Three-dimensional seismic structure and physical properties of the crust and shallow mantle beneath the East Pacific Rise at 9°30'N: Journal of Geophysical Research, v. 105, p. 23,537–23,555, doi:10.1029/2000JB900210.
- Dunn, R.A., Lekic, V., Detrick, R.S., and Toomey, D.R., 2005, Three-dimensional seismic structure of the Mid-Atlantic Ridge (35°N): Evidence for focused melt supply and lower crustal dike injection: Journal of Geophysical Research, v. 110, B09101, doi:10.1029/2004JB003473.
- Eason, D.E., Dunn, R.A., Canales, J.P., and Sohn, R., 2016, Segment-scale variations in seafloor volcanic and tectonic processes from multibeam sonar imaging, Mid-Atlantic Ridge Rainbow region (35°45′– 36°35′N): Geochemistry, Geophysics, Geosystems, v. 17, p. 3560–3579, doi:10.1002/2016GC006433.
- Garcés, M., and Gee, J., 2007, Paleomagnetic evidence of large footwall rotations associated with low-angle faults at the Mid-Atlantic Ridge: Geology, v. 35, p. 279–282, doi:10.1130/G23165A.1.
- German, C.R., and Parson, L.M., 1998, Distributions of hydrothermal activity along the Mid-Atlantic

- Ridge: Interplay of magmatic and tectonic controls: Earth and Planetary Science Letters, v. 160, p. 327–341, doi:10.1016/S0012-821X (98)00093-4.
- German, C.R., Parson, L.M., and Team, H.S., 1996, Hydrothermal exploration near the Azores Triple Junction: Tectonic control of venting at slowspreading ridges: Earth and Planetary Science Letters, v. 138, p. 93–104, doi:10.1016/0012 -821X(95)00224-Z.
- German, C.R., Thurnherr, A.M., Knoery, J., Charlou, J.-L., Jean Baptiste, P., and Edmonds, H.N., 2010, Heat, volume and chemical fluxes from submarine venting: A synthesis of results from the Rainbow hydrothermal field, 36°N MAR: Deep-Sea Research, v. 57, p. 518–527, doi:10.1016/j.dsr .2009.12.011.
- Grimes, C.B., John, B.E., Cheadle, M.J., and Wooden, J.L., 2008, Protracted construction of gabbroic crust at a slow spreading ridge: Constraints from <sup>206</sup>Pb/<sup>238</sup>U zircon ages from Atlantis Massif and IODP Hole U1309D (30°N, MAR): Geochemistry, Geophysics, Geosystems, v. 9, Q08012, doi: 08010.01029/02008GC002063.
- Holm, N.G., and Charlou, J.L., 2001, Initial indications of abiotic formation of hydrocarbons in the Rainbow ultramafic hydrothermal system, Mid-Atlantic Ridge: Earth and Planetary Science Letters, v. 191, p. 1–8, doi:10.1016/S0012-821X(01) 00397-1.
- Humphris, S.E., and Cann, J.R., 2000, Constraints on the energy and chemical balances of the modern TAG and ancient Cyprus seafloor sulfide deposits: Journal of Geophysical Research, v. 105, p. 28,477–28,488, doi:10.1029/2000JB900289.
- Kelemen, P.B., and Aharonov, E., 1998, Periodic formation of magma fractures and generation of layered gabbros in the lower crust beneath oceanic spreading ridges, in Buck, W.R., et al., eds., Faulting and magmatism at mid-ocean ridges: American Geophysical Union Geophysical Memoir 106, p. 267–289, doi:10.1029/GM106p0267.
- Kuznetsov, V., Cherkashev, G., Lein, A., Shilov, V., Maksimov, F., Arslanov, K., Stepanova, T., Baranova, N., Chernov, S., and Tarasenko, D., 2006, <sup>230</sup>Th/U dating of massive sulfides from the Logatchev and Rainbow hydrothermal fields (Mid-Atlantic Ridge): Geochronometria, v. 25, p. 51–55.
- Lartaud, F., et al., 2010, Fossil clams from a serpentinite-hosted sedimented vent field near the active smoker complex Rainbow, MAR, 36°13′N: Insight into the biogeography of vent fauna: Geochemistry, Geophysics, Geosystems, v. 11, Q0AE01, doi:10.1029/2010GC003079.
- Lartaud, F., Little, C.T.S., de Rafaelis, M., Bayon, G., Dyment, J., Ildefonse, B., Gressier, V., Fouquet, Y., Gaill, F., and Le Bris, N., 2011, Fossil evidence for serpentinzation fluids fueling chemosynthetic assemblages: Proceedings of the National Academy of Sciences of the United States of America, v. 108, p. 7698–7703, doi:10.1073/pnas.1009383108.

- MacLeod, C.J., Searle, R.C., Murton, B.J., Casey, J.F., Mallows, C., Unsworth, S.C., Achenbach, K.L., and Harris, M., 2009, Life cycle of oceanic core complexes: Earth and Planetary Science Letters, v. 287, p. 333–344, doi:10.1016/j.epsl.2009.08.016.
- Marjanović, M., Carbotte, S., Carton, H., Nedimović, M.R., Mutter, J.C., and Canales, J.P., 2014, A multi-sill magma plumbing system beneath the axis of East Pacific Rise: Nature Geoscience, v. 7, p. 825–829, doi:10.1038/ngeo2272.
- Marques, A.F.A., Barriga, F.J.A.S., and Scott, S.D., 2007, Sulfide mineralization in an ultramafic-rock hosted seafloor hydrothermal system: From serpentinization to the formation of Cu-Zn-(Co)rich massive sulfides: Marine Geology, v. 245, p. 20–39, doi:10.1016/j.margeo.2007.05.007.
- Nedimović, M.R., Carbotte, S.M., Harding, A.J., Detrick, R.S., Canales, J.P., Diebold, J.B., Kent, G.M., Tischer, M., and Babcock, J., 2005, Frozen magma lenses below the oceanic crust: Nature, v. 436, p. 1149–1152, doi:10.1038/nature03944.
- O'Hanley, D.S., 1992, Solution to the volume problem in serpentinization: Geology, v. 20, p. 705–708, doi:10.1130/0091-7613(1992)020<0705: STTVPI>2.3.CO;2.
- Okino, K., Nakamura, K., and Sato, H., 2015, Tectonic background of four hydrothermal fields along the Central Indian Ridge, in Ishibashi, J. I., et al., eds., Subseafloor biosphere linked to hydrothermal systems—TAIGA Concept: Tokyo, Japan, Springer, p. 133–146, doi:10.1007/978-4-431-54865-2\_11.
- Ondreas, H., Cannat, M., Fouquet, Y., and Normand, A., 2012, Geological context and vents morphology of the ultramafic-hosted Ashadze hydrothermal areas (Mid-Atlantic Ridge 13°N): Geochemistry, Geophysics, Geosystems, v. 13, Q0AG14, doi:10.1029/2012GC004433.
- Paulatto, M., Canales, J.P., Dunn, R.A., and Sohn, R.A., 2015, Heterogeneous and asymmetric crustal accretion: New constraints from multi-beam bathymetry and potential field data from the Rainbow area of the Mid-Atlantic Ridge (36°15'N): Geochemistry, Geophysics, Geosystems, v. 16, p. 2994–3014, doi:10.1002/2015GC005743.
- Singh, S.C., Collier, J.S., Harding, A.J., Kent, G.M., and Orcutt, J.A., 1999, Seismic evidence for a hydrothermal layer above the solid roof of the axial magma chamber at the southern East Pacific Rise: Geology, v. 27, p. 219–222, doi:10.1130 /0091-7613(1999)027<0219:SEFAHL>2.3.CO;2.
- Tucholke, B.E., and Lin, J., 1994, A geological model for the structure of ridge segments in slow spreading ocean crust: Journal of Geophysical Research, v. 99, p. 11,937–11,958, doi:10.1029/94JB00338.

Manuscript received 12 November 2016 Revised manuscript received 21 January 2017 Manuscript accepted 27 January 2017

Printed in USA